Bioresource Technology 462 (2026) 135510

Contents lists available at ScienceDirect

Bioresource Technology

journal homepage: www.elsevier.com/locate/biortech

The extremophile *Chlamydomonas acidophila* PM01 survives high manganese contamination by restricting non-vacuolar intracellular content

Isidora Santrač [a], Milena Dimitrijević [a], Milan Žižić [a,b], Marina Stanić [a], Valentina Ćurić [a], Valentina Bonanni [b], Alessandra Gianoncelli [b], Giuliana Aquilanti [b], Chiaramaria Stani [b], Giovanni Birarda [b], Wilfred Hagen [c], Uroš Javornik [d], Bernd Zechmann [e], Jon K. Pittman [f], Ivan Spasojević [a,*], Jelena Danilović Luković [a]

[a] University of Belgrade - Institute of Multidisciplinary Research, National Institute of the Republic of Serbia, Belgrade, Serbia
[b] Elettra Sincrotrone Trieste S.C.p.A., Basovizza, Trieste, Italy
[c] Department of Biotechnology, Delft University of Technology, Delft, the Netherlands
[d] Slovenian NMR Center, National Institute of Chemistry, Hajdrihova 19, 1000 Ljubljana, Slovenia
[e] Center for Microscopy and Imaging, Baylor University, Waco, TX, USA
[f] Department of Earth and Environmental Sciences, School of Natural Sciences, The University of Manchester, Manchester, UK

HIGHLIGHTS

- Microalga *Chlamydomonas acidophila PM01* tolerates extremely high Mn levels.
- Cells do not accumulate large amounts of Mn.
- Mn is bound to the cell wall and coordinated by phosphates in vacuoles and excreted.
- *C. acidophila* could be used for biomass production in Mn-infested waters.
- Acidophilic microalgae show Mn exclusion tolerance strategy.

GRAPHICAL ABSTRACT

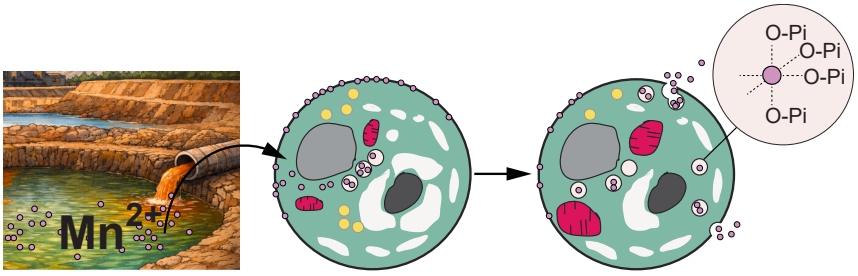

ARTICLE INFO

Keywords:
Acid mine drainage
Extremophile
Mn sequestration
Tolerance
Vacuolar metal homeostasis

ABSTRACT

Acidophilic and metallotolerant microalgae represent an indispensable element of strategies to exploit or revive acid mine drainage ponds and similar systems with high levels of dissolved metal ions. The selection of an optimal strain for a specific application depends on the capacity to tolerate selected metal(s) and on the mechanisms of tolerance. Herein we examined the tolerance to manganese by *Chlamydomonas acidophila* PM01, an extremophilic strain that lives under acidic conditions and high concentrations of iron and other metals in its anthropogenic aquatic habitat. PM01 survived an extremely high Mn concentration of 50 mM (2.75 g/L). At 20 mM, cells kept intracellular Mn concentrations at a low level probably through binding to the cell wall, and vacuolization and excretion of Mn from the cell. Mn^{2+} was sequestrated by oxygen ligands, including phosphates, in octahedral geometry, in vacuoles and the cell wall. Energy challenges induced by Mn excess are met by the consumption of starch and lipid reserves, and improved photosynthetic performance. The exposure to Mn excess was related to decreased abundance of Fe-metalloenzymes and mild oxidative stress. The tolerance to Fe is

* Corresponding author at: University of Belgrade – Institute for Multidisciplinary Research, National Institute of the Republic of Serbia, Kneza Višeslava 1, 11000 Belgrade, Serbia.
E-mail address: ivan@imsi.bg.ac.rs (I. Spasojević).

https://doi.org/10.1016/j.biortech.2026.135510
Received 3 April 2026; Received in revised form 12 July 2026; Accepted 26 July 2026
Available online 27 July 2026

coincident to tolerance to Mn. Acidophilic microalgae may be used for commercialization of metal-infested waters through biomass and biofuels production avoiding the need to use freshwaters and reducing contamination by other organisms. Finally, our study points out a novel low-intracellular Mn retention tolerance model that may be specific to acidophilic eukaryotic microalgae and enable superior survival tolerance. However, such strategy of tolerance is not optimal for bioremediation.

1. Introduction

Manganese (Mn) is a common and important pollutant of wastewaters from Mn mining, ore processing and electrolytic Mn production (Li et al., 2019; Neculita and Rosa, 2019). Such acidic wastewaters are recognized geochemical hotspots of Mn mobilization, releasing dissolved Mn to adjacent groundwaters and surface waters (Kossoff et al., 2014). Although Mn is not one of the most dangerous pollutants, it is a widespread ecotoxicological and health threat (Dey et al., 2023). On the other hand, it is an important essential micronutrient of particular interest to photosynthetic organisms, including microalgae which can opportunistically accumulate Mn beyond its metabolic quota (Blaby-Haas and Merchant, 2012; Saha et al., 2013). Mn is 'notoriously' hard to remove from wastewaters, in part because it is soluble at high pH values (up to pH 8), which constitutes a limitation to metal precipitation approaches in water treatment (Neculita and Rosa, 2019). It is present in waters in the Mn^{2+} redox form with reduction potentials that are too high to allow 'spontaneous' redox activity and the production of reactive oxygen species (ROS), which is typical for Cu and Fe. However, Mn^{2+} can be oxidized by some microorganisms, including microalgae, to Mn^{3+} and Mn^{4+} (Tanović et al., 2025; Vojvodić et al., 2023). These redox forms are not stable and may promote the production of free radicals and oxidative stress which has been related to Mn toxicity in microalgae (Li et al., 2007; Nowicka, 2022). On the other hand, Mn excess may also result in the mis-metallation of Fe-enzymes with significant metabolic consequences (Imlay, 2014).

Chlamydomonas acidophila is an extremophilic green microalga well-adapted to thrive in acidic environments, such as acid mine drainage (AMD) ponds and rivers (Dean et al., 2019; Olsson et al., 2015; Puente-Sánchez et al., 2018). Low pH promotes metal leaching from mining debris and sediment so acidic waters commonly contain high levels of dissolved metal ions. *C. acidophila* is one of a small number of Eukaryotic microorganisms that can colonize and restart biological activity in such acidic and metal contaminated systems (Nixdorf et al., 1998; Ňancucheo and Johnson, 2011). Previous studies have examined the mechanisms that enable *C. acidophila* to tolerate excess of some metals that may be present in AMD environments, such as iron (Fe), copper (Cu), zinc (Zn) and cadmium (Dean et al., 2019; Olsson et al., 2015; Puente-Sánchez et al., 2018). However, there have been no investigations to date on the tolerance of this microalga to Mn. Understanding the mechanisms of tolerance is essential for optimizing the use of *C. acidophila* in waters where this metal represents a barrier to other organisms. The key bifurcation is between the use of extremophilic microalgae in bioremediation of wastewaters, which requires strains that can sequester significant amounts of Mn, and their use as a potential means to produce biomass in wastewaters. So far this second concept is largely unexplored, but it can alleviate the problem of limited access to freshwater through commercial exploitation of polluted waters in the production of biomass, which preferably should not be contaminated by metals such as Mn (Wollmann et al., 2019).

The current study addressed the mechanism of Mn tolerance of *C. acidophila* strain PM01. This strain has previously been isolated from one of the AMD ponds at the Parys Mountain mining site in the UK (Dean et al., 2019; Mcintosh, 2021). The exploitation of the mine ended in the early 1900 s, but the site still represents a considerable environmental threat. The water in the pond has pH of ~1.5 (other nearby AMD ponds that contain the microalga have pH ranges of 2 to 5), and approximately 20 mM of dissolved metal ions, including Fe (15 mM), Al (2.5 mM), Cu (1 mM), and Zn (0.5 mM). It is important to note that the measured dissolved Mn concentration in the pond was low and typically did not exceed 20 μM and reached up to 150 μM at other AMD ponds at the site (Dean et al., 2019). Pertinent to this, the aim of this study was also to resolve whether the natural tolerance to high Fe transposes to tolerance to high concentrations of Mn which is not a challenge in the native anthropogenic habitat. The metabolisms of Fe and Mn are intertwined (Blaby-Haas and Merchant, 2012). For example, it has been shown that Mn may partially relieve the effects of Fe limitation on microalgal growth (Liu et al., 2018). Previous analyses showed that PM01 strain can tolerate 15 mM Zn and 1.5 mM Cu, when grown in pH 3 conditions, without a significant impact on growth rate. It has been proposed that the mechanisms behind the tolerance to Cu excess include metabolic changes, upregulation of antioxidative defense, alterations in photosynthetic performance, and some metal bioaccumulation through internalization (Dean et al., 2019; Mcintosh, 2021).

2. Methods and materials

2.1. Cell cultures and treatment

C. acidophila PM01 strain was kindly provided by Jon Pittman at the University of Manchester. The strain had been isolated from AMD ponds at the abandoned Parys Mountain mine site, Anglesey, North Wales, UK (Dean et al., 2019). Microalgae were grown under photoautotrophic conditions in an optimal, nutrient-sufficient modified MAM medium (initial pH = 3) (Canadian Phycological Culture Centre, 2026; Olaveson and Stokes, 1989). This pH has been used previously as optimal for the growth of PM01 strain (Dean et al., 2019). Microalgal inoculums were added to 150 mL of MAM medium in 250 mL Erlenmeyer flasks, at an initial density of 5×10^5 cells/mL. Microalgae were grown at 22 °C on orbital shakers (120 rpm) in a growth cabinet with a continuous photon flux of 120 μmol m^{-2} s^{-1} (MST TL-D Reflex 36 W840 1 SLV/25 tubes, Philips, Amsterdam, The Netherlands). Flasks with samples were weighed on day 0 and the volume of samples was corrected for evaporation on day 10 with sterile deionized water (5–8 mL). The culture's growth was monitored by optical density at 750 nm (OD_{750}), biomass (dry biomass per mL), viability, and cell count. To determine biomass, 2 mL aliquots were washed with water, centrifuged at 5000 g / 5 min, and the pellets were left to dry at 60 °C for 24 h. Cell viability was assessed by Evans Blue staining. The viability is reported as the percentage of Evans Blue-negative cells (Zuppini et al., 2007). Cell count was carried out using a Sedgewick-Rafter counting chamber. For this purpose, cells were stained with Lugol's iodine solution (100 μL per mL of sample). Cell cultures were treated at day 15. To determine the tolerance of the strain, the culture was exposed to varying concentrations of $MnCl_2$ (in the form of $MnCl_2 \times 4\ H_2O$) ranging from 2 mM to 200 mM. Since PM01 tolerated very high Mn concentrations, all further experiments were performed using a Mn^{2+} concentration of 20 mM which resembles the concentration of dissolved metal ions in its native anthropogenic habitat. The exception was for methods that could suffer from changes in the bulk magnetic susceptibility, such as EPR and NMR, and so a lower Mn^{2+} concentration (2 mM) was used. The accumulation of Mn in the biomass was established using an inductively coupled plasma optical emission spectrometry (ICP-OES) spectrometer (Avio 200, PerkinElmer, 143 Waltham, MA, USA). Microalgae culture samples (150 mL) obtained from different time points after treatment with 2 mM or 20 mM $MnCl_2$ and corresponding controls were washed three times with 50 mL of

deionized water and centrifugation at 5000 g for 5 min. Biomass was collected and dried for 24 h at 60 °C. Biomass (30 mg samples) was digested using a mixture of 8 mL 65 % HNO_3 and 2 mL 30 % H_2O_2. Digestion was performed at 120 °C for 30 min. The concentration of Mn in the medium was measured using colorimetric determination of Mn with KIO_4 (Marczenko and Balcerzak, 2000). Briefly, microalgal cultures were treated with 20 mM $MnCl_2$. pH of the samples was ~2.3. Samples (2 mL) were collected over a period of 24 h. Supernatants from untreated culture was supplemented with 20 mM $MnCl_2$ to prepare control samples. Samples were centrifuged at 10,000 g for 5 min to collect supernatant (1.6 mL) that was digested with 8 mL of 65 % HNO_3 and 2 mL of 30 % H_2O_2 for 30 min at 120 °C. Digested sample was diluted 3 × and 0.6 mL were mixed with 1.4 mL of 15 mM KIO_4 in 0.5 M HNO_3. The mixture was heated in 10 mL glass beakers to approximately 70 °C until the stabilization of purple color was achieved (10–15 min). After cooling, the mass of the sample was adjusted. The absorbance of samples was measured using a 96-well plate on a Tecan Infinite M Nano microplate reader (Tecan Group Ltd, Männedorf, Switzerland) at 524 nm. The detection limit of the method was 2 μM.

All chemicals were acquired from Merck (Darmstadt, Germany), unless stated differently. For additional methods – scanning electron microscopy (SEM), starch content assay, and Nile Red assay for relative lipid content, see Supplementary Information.

2.2. Low energy micro-X-ray fluorescence microscopy (LE-μXFM)

For synchrotron radiation-based LE-μXFM coupled with scanning transmission X-ray microscopy (STXM), cultures were treated with 20 mM $MnCl_2$ and collected after 24 h or 72 h, or were untreated and collected at 0 h. Cultures were washed once with water, and 10 μL suspensions were placed on silicon–nitride membrane (Silson, Southam, UK) and left overnight at room temperature to dry. LE-μXFM micrographs were collected at the TwinMic beamline of Elettra Sincrotrone Trieste (Gianoncelli et al., 2016; Gianoncelli et al., 2021). Measurements were performed under the high vacuum. The samples were illuminated with a primary beam energy of 1.59 keV and raster-scanned with the 400 nm step size. The energy used for experiments was selected to excite the Na and Mg K-electrons too, since their distributions were supposed to give an indication about the location(s) of Mn in cells. LE-μXFM maps were collected by using 8 Silicon Drift Detector (SDD) detectors regularly attached in an annular configuration around the sample plane (Gianoncelli et al., 2021). Simultaneously, the transmission X-ray detector system consisted of a fast read-out CCD camera coupled with a visible light converting system used to assess the density and morphologies of control and treated cells by producing contrast images generated by the absorption and scattering of X-rays from the sample (Gianoncelli et al., 2006). Python-based open-source package, PyMCA (Solé et al., 2007), was used for processing the spectra from each pixel and producing the distribution of detected elements in each map. X-ray maps were plotted with XRFitVis web application (Kourousias et al., 2026).

2.3. X-ray absorption near edge structure (XANES) spectroscopy

The structural properties of Mn were examined using XANES spectroscopy. The experiments were conducted at an IAEA multi-technique X-ray spectrometry experimental station installed at the Elettra Sincrotrone Trieste (Trieste, Italy) synchrotron facility (Karydas et al., 2018). Samples obtained from untreated, and cultures treated with 20 mM $MnCl_2$ for 24 h and 48 h, were washed 3 × with water, freeze-drying overnight, grounded into powder, and mixed with polyvinylpyrrolidone to adjust the edge jump. Spectra were collected in the energy range from 6520–6700 eV with different step sizes in pre-edge, edge and post-edge region by a RaySpec 3-elements SIRIUS SDD. Samples were mounted in the ultra-high vacuum chamber of the beamline end station and spectra were collected in fluorescence mode. The energy scale was calibrated using the maximum of the first derivative of the K-edge absorption spectrum of an internal reference of Mn metallic foil. The XANES spectrum of several Mn reference standards was also recorded for comparison. The analysis of XANES spectra was performed using the ATHENA software package (Ravel and Newville, 2005). Before analysis, the data were processed, which included the determination of the main edge energy (E_0), background removal, and normalization of the energy jump to 1. The E_0 value was derived from the first derivative peak of the normalized spectra.

2.4. ^{31}P nuclear magnetic resonance (NMR)

^{31}P NMR spectroscopy was applied to elucidate the interactions of paramagnetic Mn^{2+} with (poly)phosphates. Microalgal samples (150 mL) were untreated, or treated with 2 mM $MnCl_2$ for 24 h. It is important to note that 2 mM Mn^{2+} instead of 20 mM was applied here and in low-T EPR experiments to avoid changes in bulk magnetic susceptibility. Cells were centrifuged at 5000 *g* for 5 min, washed twice with and resuspended in 0.1 M citrate buffer pH = 3. Fresh samples were prepared just prior to the measurements. Washed cells were suspended in 0.5 mL of citrate buffer containing $NaHCO_3$ (1 mM). The resulting suspensions were placed in 5 mm NMR tubes. ^1H decoupled ^{31}P NMR spectra were acquired at 298 K on a Bruker Avance NEO 600 MHz NMR spectrometer tuned at the ^{31}P resonance frequency using a 90° pulse with a 5 s repetition rate (relaxation delay + acquisition time), 8192 points, 17241 Hz (71.0 ppm) spectra width, and an offset of 15.0 ppm. Spinning rate was set to 20 Hz. A total of 1420 scans were acquired for each spectrum. In addition, pH dependence of the shift of orthophosphate line was established by collecting spectra of 1 mM H_3PO_4 in water at different pH values, using the same experimental setting, acquiring 16 scans per spectrum. All spectra were referenced externally against 85 % H_3PO_4. Signals were processed, analyzed, and deconvoluted in Topspin 4.5.0. (Bruker).

2.5. Electron paramagnetic resonance spectroscopy (EPR) of Mn

EPR measurements were performed on biomass of *C. acidophila* PM01 cultures exposed to 2 mM $MnCl_2$ for 24 h or 72 h, using a Bruker EMXplus EPR spectrometer operating in X- band (9.41 GHz) at temperatures between 15.5 K and 293 K, using the following conditions: attenuation, 26 dB (15.5 K) to 4 dB (293 K); modulation amplitude, 0.5 mT; modulation frequency, 100 kHz; scan time 100 s. The signals were checked for absence of saturation. EPR signals were corrected for temperature and plotted versus the temperature to gain additional information on the spin and to estimate ground/excited state separation.

2.6. Transmission electron microscopy (TEM)

Cell aliquots from controls (collected at 0 h) and cultures that were treated with 20 mM $MnCl_2$ and collected after 24 h or 48 h, were spun down at 5000 g for 5 min, and fixed overnight at 4 °C in 2.5 % glutaraldehyde (v/v) in 0.1 M phosphate buffer (PB; pH = 7.2; Serva, Heidelberg, Germany). Post-fixation was performed using 1 % (w/v) osmium tetroxide (pH = 7.2, Serva) in 0.1 M PB for 2 h at room temperature. After dehydration in a graded acetone series (50 %, 70 %, 90 %, and 100 %) samples were infiltrated with mixtures of acetone:Agar 100 resin (AGR1031, Agar Scientific, Stansted, UK): 2/1 for 1 h, 1/1 for 1 h, 2/1 overnight, and 100 % for 4 h, and polymerized in resin for medium blocks (AGR1031, Agar Scientific) at 60 °C for 48 h. Resin blocks were trimmed and ultra-thin sections (70 nm) were sectioned using an EM UC7 ultramicrotome (Leica Microsystems, Wetzlar, Germany). Ultra-thin sections were post-contrasted with lead citrate (1 % dissolved in 0.6 M NaOH) for 5 min and uranyl-acetate (2 % dissolved in water) for 15 min. Post-contrasted sections were imaged in STEM-HAADF mode according to Haberman et al. (2025), with a Spectra 300C TEM (Thermo Fisher Scientific, Hillsboro, OR, USA), with the

following settings: energy, 300 KeV; spot size, 4; resolution, 2048 × 2048; dwell time, 10 μs. Morphometric analyses were performed using Image J (NIH). All measurements were conducted by hand-selected analysis of > 25 cells at × 8000 magnification.

2.7. Synchrotron radiation Fourier transform mid-infrared spectromicroscopy (SR-μFTIR)

SR-μFTIR measurements were performed at the SISSI-Bio Beamline at Elettra Sincrotrone Trieste (Birarda et al., 2022). Microalgal samples from untreated (obtained at 0 h) and cultures treated with 20 mM $MnCl_2$ after 24 h or 72 h were prepared as for LE-μXFM. After washing, 10 μL of microalgae cell suspension was placed on silicone-nitride membrane (Silson), and left overnight at room temperature to dry in air. FTIR measurements were carried out using an IR/VIS microscope (Hyperion 3000, Bruker Optics, Billerica, MA, US) coupled with an in-vacuum benchtop interferometer (VERTEX70 V, Bruker Optics, Billerica, MA, US). The microscope was equipped with 15 × objective and a single point MCT Detector (Infrared Associates Inc. STUART, FL, US). The spectra were acquired in the spectral range 4000–600 cm^{-1} at spectral resolution 4 cm^{-1} averaging 256 scans. For each treatment ~30 independent spectra were collected, by closing the apertures at 20x20 microns and measuring small groups of cells. The acquired data were corrected for water vapor using a built-in routine of OPUS 8.5 SP1 (Bruker Optics Billerica, MA, US) and then analyzed with QUASAR open-source software (Toplak et al., 2017; Toplak et al., 2021). In QUASAR, the data were pre-processed (cut and baseline corrected using rubber-band function) and the integrals were calculated. The bands were identified based on previously published FTIR data for microalgae (Dean et al., 2019; Driver et al., 2015). The level of lipid peroxidation was calculated using the =C-—H/total lipids ratio that was estimated by the ratio of intensities of FTIR signal in the 2997–3024 cm^{-1} range and 2800–3000 cm^{-1} range. Lipid peroxidation is reciprocally proportional to this ratio (Movasaghi et al., 2008). Protein oxidation was estimated by the level of carbonyl groups that was determined by the intensity of FTIR signal in the 1710–1770 cm^{-1}.

2.8. Redox parameters

The intracellular concentration of ROS was evaluated using dichlorodihydrofluorescein diacetate (DCFH-DA), as described previously (Kalyanaraman et al., 2012). Aliquots of culture samples (untreated or treated with 20 mM $MnCl_2$; were washed 3 × and diluted with water to set OD_{750} at ~0.5. DCFH-DA was dissolved in 96 % ethanol and added to the samples at the final concentration of 20 μM (final ethanol concentration was 1 %). After incubation in the dark for 20 min at 25 °C, samples (200 μL) were placed in microtiter plates (black walls/clear bottom). DCFH fluorescence was read on a Tecan Infinite M Nano microplate reader, with 485 nm excitation and 530 nm emission. The obtained results are presented in arbitrary units, and corrected by autofluorescence of microalgae and fluorescence of DCFH-DA (Kalyanaraman et al., 2012).

X-band EPR spectroscopy with disulfide biradical (RSSR) method was used to determine the levels of reduced thiol groups (Khramtsov et al., 1989). Aliquots were collected from untreated cultures (at 0 h and 24 h) or cultures exposed to 2 mM and 20 mM $MnCl_2$ (at different time points between 15 min and 24 h), washed 3 × and diluted in water to a final number of 2×10^6 cells per 50 μL samples. After incubation of samples with 100 μM RSSR spin probe (Enzo Life Sciences, Farmingdale, NY, USA) for 10 min, EPR spectra were collected at room temperature on Bruker EMX Nano Spectrometer. The settings were: attenuation, 20 dB; modulation amplitude, 0.1 mT; modulation frequency, 100 kHz; scan time, 60 s.

2.9. Western blot of antioxidative enzymes

Culture samples were washed with water and snap-frozen in liquid N_2. Samples were homogenized upon thawing on ice in 50 mM potassium phosphate buffer (pH = 7, with 0.4 % Triton X-100) in 1:4 mass ratio using an ultrasonic homogenizer (6 × 5 s mixing at 26 Hz). Homogenates were further gently shaken on ice for 60 min with 10 s vortex every 15 min, and centrifuged at 16,000 g/30 min/4 °C. Protein-containing supernatants were collected and incubated with Laemmli buffer for 10 min at 95 °C, resolved on a 10 % SDS-polyacrylamide gel, and transferred to a PVDF membrane. After blocking with bovine serum albumin (5 %), blots were incubated with primary antibodies (Agrisera, Vännäs, Sweden): catalase (CAT; AS15 2991), chloroplastic iron-dependent superoxide dismutase (FeSOD; AS06 125), and manganese SOD (MnSOD; AS21 4523), and secondary goat anti-rabbit antibody conjugated with horseradish peroxidase (ab6721; Abcam, Cambridge, UK). Visualization was performed using iBright™ FL1500 Imager (Thermo Fisher Scientific). Band intensities were normalized to loading control (GAPDH; FNab03342, Fine Test, Wuhan, China).

2.10. PAM fluorimetry

Fluorescence measurements were performed on a Mini PAM II/R fluorimeter (Heinz Walz GmbH, Effeltrich, Germany). Microalgal culture treated with 20 mM $MnCl_2$ for 1 h, 24 h, or 48 h, and corresponding controls (untreated, sampled at 0 h) were washed 3 × with water (cell density ~4 × 10^7 cells/mL). Samples were supplemented with 2 mM $NaHCO_3$ to ensure that electron transport was not limited by the carbon supply (Cazzaniga et al., 2014). Concentrated culture (0.5 mL) was placed in a suspension cuvette, stirred and kept in the dark for 15 min prior to measurements.

The maximum quantum efficiency of photosystem II (PSII), expressed as Fv/Fm ratio was assessed by applying saturating pulse (intensity: ~6000 μmol photons m^{-2} s^{-1}, width: 1 s) preceded by 5 s of far-red light. Rapid light curve (RLC) was used to determine the effective photochemical yield (Y(II)), non-photochemical quenching (NPQ) and the electron transport rate (ETR). RLC parameters were: 10 distinct irradiance levels, 10 s width, each ending with saturating pulse. ETR was fitted according to Platt et al. for estimation of ETRmax and Ik parameters (Platt et al., 1980). All analyses were conducted following the procedures described by Walz (Walz, 2000).

2.11. Statistics

All experiments were conducted with a minimum of three biological replicates and the results are expressed as means ± standard error (SE). The numbers of exact biological (n) replicates are provided in figure legends. Statistical analysis was performed using Sigma Plot 12.3 (Systat Software Inc., San Jose, California, USA). For comparisons between control and treated microalgae, the Mann–Whitney 2-tailed test was used. The level of statistical difference was $p < 0.05$. Data for lipid peroxidation were represented as box plots.

3. Results and discussion

3.1. Viability and intracellular and extracellular Mn pool during exposure to high environmental Mn

Growth parameters and viability of the *C. acidophila* PM01 culture were not affected by Mn^{2+} at concentrations of up to 50 mM even after 7 days of treatment (Fig. 1). At 200 mM Mn, the viability was drastically decreased after only 1 h, with less than 20 % of cells remaining alive after 7 days. Viability in untreated samples at the day of the treatment was ~95 % (see Supplementary Information). High Mn concentrations contributed to the dry residue mass, significantly impacting biomass measurements in cultures treated with 200 mM Mn. All further analyses

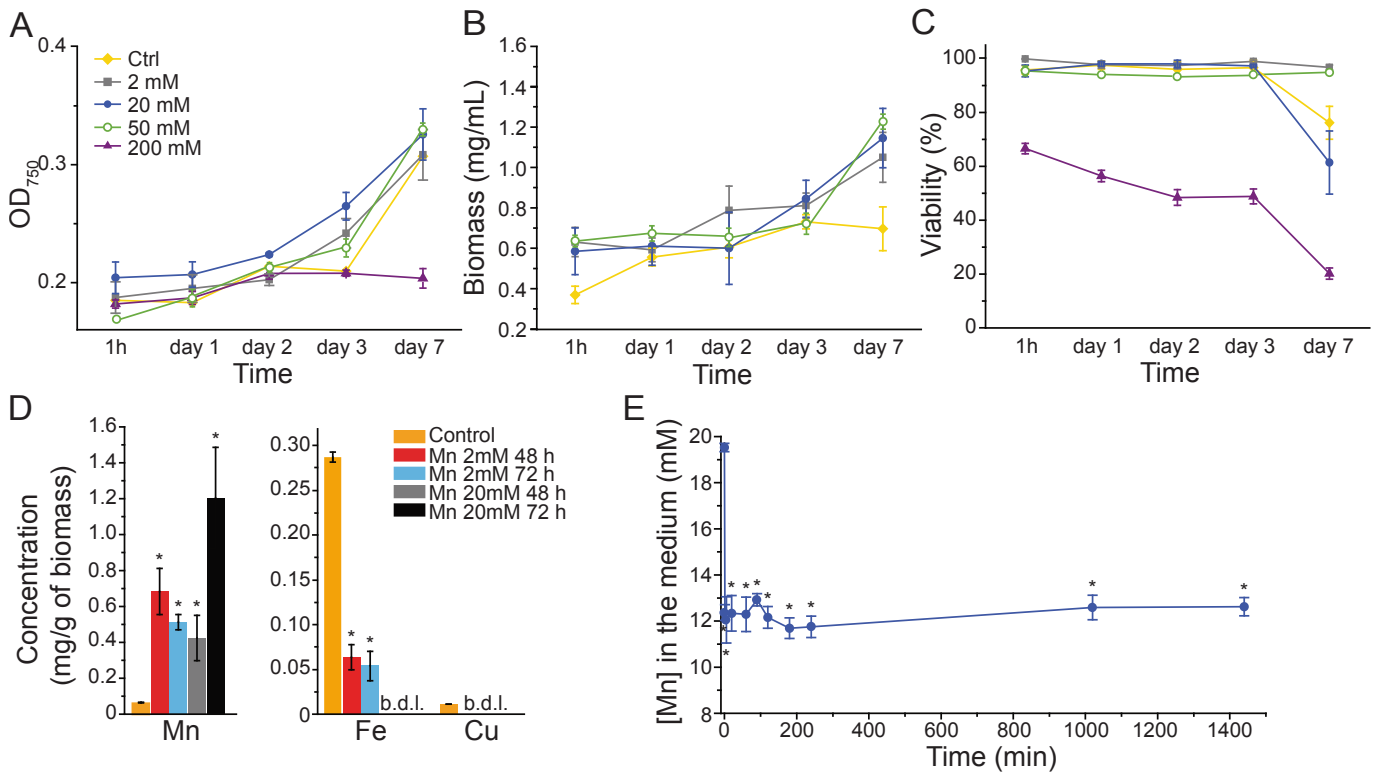

Fig. 1. Growth parameters and viability for *C. acidophila* PM01 culture and the concentration of metals in the biomass during exposure to different concentrations of $MnCl_2$. (A) Optical density at 750 nm; (B) Biomass. Data obtained for cultures treated with 200 mM Mn^{2+} are not presented. (C) Viability, determined by Evans blue assay. The viability in cultures prior to exposure to 200 mM Mn was ~100 %; The decrease in viability after 1 h and at all other timepoints was statistically significant ($p < 0.05$). $MnCl_2$ was added on the 15th day post-inoculation and the effects were monitored for 7 days. Results are presented as means ± SE (n = 8); (D) The concentration of Mn, Fe and Cu in the biomass from untreated cultures or $MnCl_2$ treated cultures. Data are presented as means ± SE (n = 5). (E) Mn concentration in the medium of cultures treated with 20 mM $MnCl_2$. Control (0 min) represents medium collected from untreated culture, supplemented with 20 mM $MnCl_2$, and further processed as other samples. Data are presented as means ± SE (n = 4). * – statistically significant compared to control ($p < 0.05$). B.d.l. – below detection limit.

were performed using 20 mM (or 2 mM for some methods). It is important to point out that the PM01 strain showed survival tolerance to 50 mM Mn (2.75 g of Mn per L; at pH = 3). To the best of our knowledge, this is more than any previously examined (eukaryotic) microalgal species (Alho et al., 2022; Cândido et al., 2024; Vasilieva et al., 2022; Vojvodić et al., 2023). In addition, this is higher than Mn levels in any industrial wastewater recorded so far in public records (we could not find higher concentration than 1.8 g/L (Shu et al., 2016)). Nevertheless, understanding maximum tolerance thresholds can be beneficial. The remarkable ability of this organism to tolerate very high concentrations of Mn as well as other metals, could be essential for cultivation in closed systems with metal contaminated waters in which, by evaporation, could easily reach very high metal concentrations. It appears that the tolerance to high Fe (and other metals) that shaped PM01 in its original habitat (Dean et al., 2019; Driver et al., 2015), extrapolates to tolerance to extreme Mn concentrations. This may be related to the overlapping transport and metabolic pathways of these metals in microalgae (Blaby-Haas and Merchant, 2012).

Low Mn absorption indicates that an important aspect of Mn tolerance by this microalga is through inhibiting metal ion accumulation. The concentration of Mn in the biomass was ~1.2 μg/mg (only ~0.1 % of biomass) even after 72 h treatment with 20 mM Mn (Fig. 1D). However, a significant drop of Mn concentration in the medium was observed almost instantly after the addition – from 20 mM to approximately 12 mM in 1 min (Fig. 1E). This is a decrease of about 440 μg of Mn per mL, which is approximately 600 × more than the amount of Mn found in the biomass collected in 1 mL of culture. Therefore, this might be explained by weak bonding of Mn^{2+} to the cell wall. After the initial change, Mn concentration in the medium was relatively stable, which implicates that PM01 swiftly activates mechanisms that regulate intracellular Mn levels. The calculated concentration factor was between 1 and 5. This is drastically lower compared to other microalgal species exposed to high Mn concentrations. For example, previous studies have found that *Chlorella sorokiniana* treated with 1 mM Mn accumulated the amount of Mn that is approximately 1 % of the biomass, with concentration factor of ~180 (Vojvodić et al., 2023); similar results were found for *Scenedesmus quadricauda* (Li et al., 2024); *Chlorella vulgaris* treated with 35 mM Mn accumulated Mn at the amount of 3.5 % of biomass (concentration factor ~18) (Smythers et al., 2019); *Thalassiosira pseudonana* treated with 10 mM Mn accumulated Mn at 5 % of biomass (concentration factor ~91) (Sim et al., 2021). In contrast to these strains, PM01 tolerance to Mn is not based on metal internalization and sequestration. Therefore, PM01 should not be a choice for remediation of Mn-rich waters since it does not remove significant amounts of metal ions. Alternative approaches, such as the application of biochars or composites, should be considered instead (Wibowo et al., 2025). It is important to note that the treatment with Mn reduced the intracellular level of Fe and apparently Cu (Fig. 1D). Mn^{2+} and Fe^{2+} share transport and metabolic pathways (Blaby-Haas and Merchant, 2012), and Mn is known to mis-metallate Fe-enzymes (Imlay, 2014). An excess of Mn may outcompete Fe (the initial concentration of Fe in MAM medium is ~17 μM) for transport and binding sites resulting in the observed loss of intracellular Fe quota.

3.2. Subcellular localization of Mn

LE-μXFM was combined with STXM to determine Mn intracellular distribution and co-localization with other detectable elements (Fig. 2).

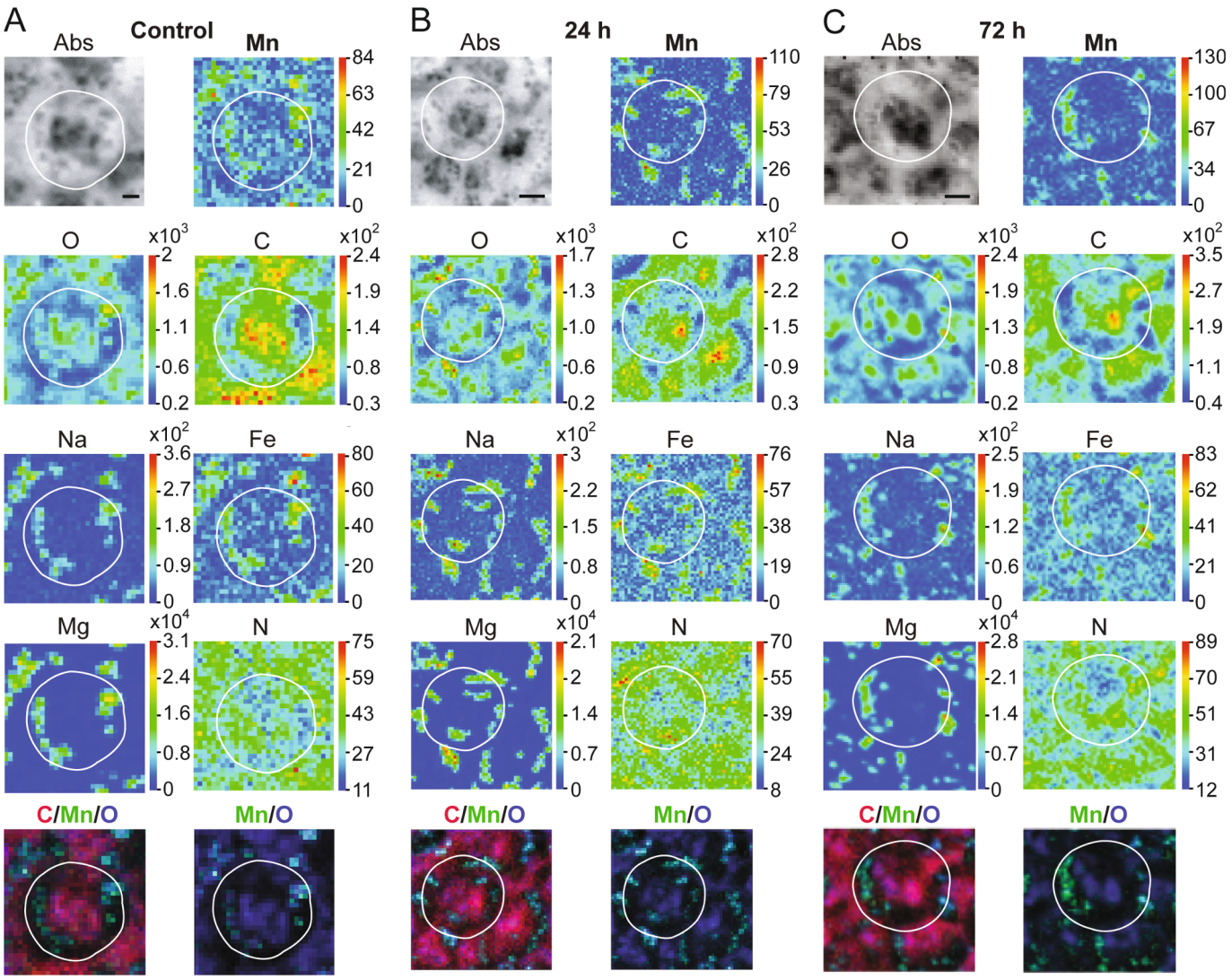

Fig. 2. Characteristic LE—μXFM and STXM absorption micrographs of *C. acidophila* PM01 cells. Cultures were: (A) untreated (control); (B) exposed to 20 mM $MnCl_2$ for 24 h; (C) exposed to 20 mM $MnCl_2$ for 72 h (n = 3). Pseudo-color scale bars represent relative concentrations of elements according to the number of counts per unit area 0.15 × 0.15 μm with dwell time of 6 s and detection time of 20 ms. Abs-X-ray phase contrast imaging enabled to define the cell boundaries. Selected overlay maps are presented in two (Mn/O (green/blue)) or three (C/Mn/O (red/green/blue)) color representations. Bar-1 μm. The central cell in the micrograph is marked with freehand outline.

The applied method enabled us to gain an insight into the distribution of light, biologically important elements – C, O, Mg, N, Na, and Fe and to correlate their distribution with Mn. The shape of the cells was clearly outlined in absorption images. Dark material-dense areas overlap with regions with high C concentrations that represent starch granules. Around this region, there are areas with high Mg, Fe and N, and Na and O that probably represent chloroplast and vacuoles (Long et al., 2023; Tanović et al., 2025). It is important to note one specific limitation of the method related to Mn. In the soft X-ray regime, the emission energies of L-lines of Mn and Fe are very close (see Supplementary Information). Since cells contain only traces of these metals, it is hard to achieve resolvable delineation between Fe and Mn L-lines in controls. Only in cells treated for 72 h, L-lines of Mn start to appear as a sign of accumulation, which made the analysis more trustable. According to it, Mn is well co-localized with Mg, Na and Fe. Regions with high C concentrations show low Mn (and Mg and Na), and *vice versa*. Further, Mn overlapped with O areas which were not overlapped with C. These areas were located around the nucleus and at the periphery of the cell. This implies that Mn is accumulated in vacuoles since these organelles show high levels of oxygen in relation to the accumulation of organic acids (Shanab et al., 2012). Vacuoles are known to act as sinks for cations, including Mn^{2+}, Mg^{2+} and Na^{+} (Blumwald et al., 2000; Pittman, 2005). In control cells, Mn was more evenly distributed throughout the cell in relation to its presence in the chloroplast (Schmollinger et al., 2023).

3.3. Coordination of Mn in cells

XANES analysis showed that Mn after entering the cell remained in the 2 + redox state (Fig. 3A, B). The comparison with XANES spectra of standard compounds suggested local coordination resembling Mn surrounded by O ligands. The overlap of pre-edge features between the treated microalgae and reference standards indicates that Mn^{2+} in biomass has an octahedral coordination environment. Of note, XANES spectrum of Mn in the biomass was clearly different to the spectrum of $MnCl_2{\cdot}4H_2O$ which was used to supplement Mn^{2+} to the cell culture (Fig. 3B). ^{31}P NMR spectroscopy was applied to examine whether that Mn^{2+} ions are coordinated by (poly)phosphates (Fig. 3C). Manganese ions are paramagnetic and relaxation agents that cause broadening of spectral lines of their ligands (Lacerda et al., 2021). ^{31}P NMR spectrum is in accord with previous NMR reports on other strains of *C. acidophila*,

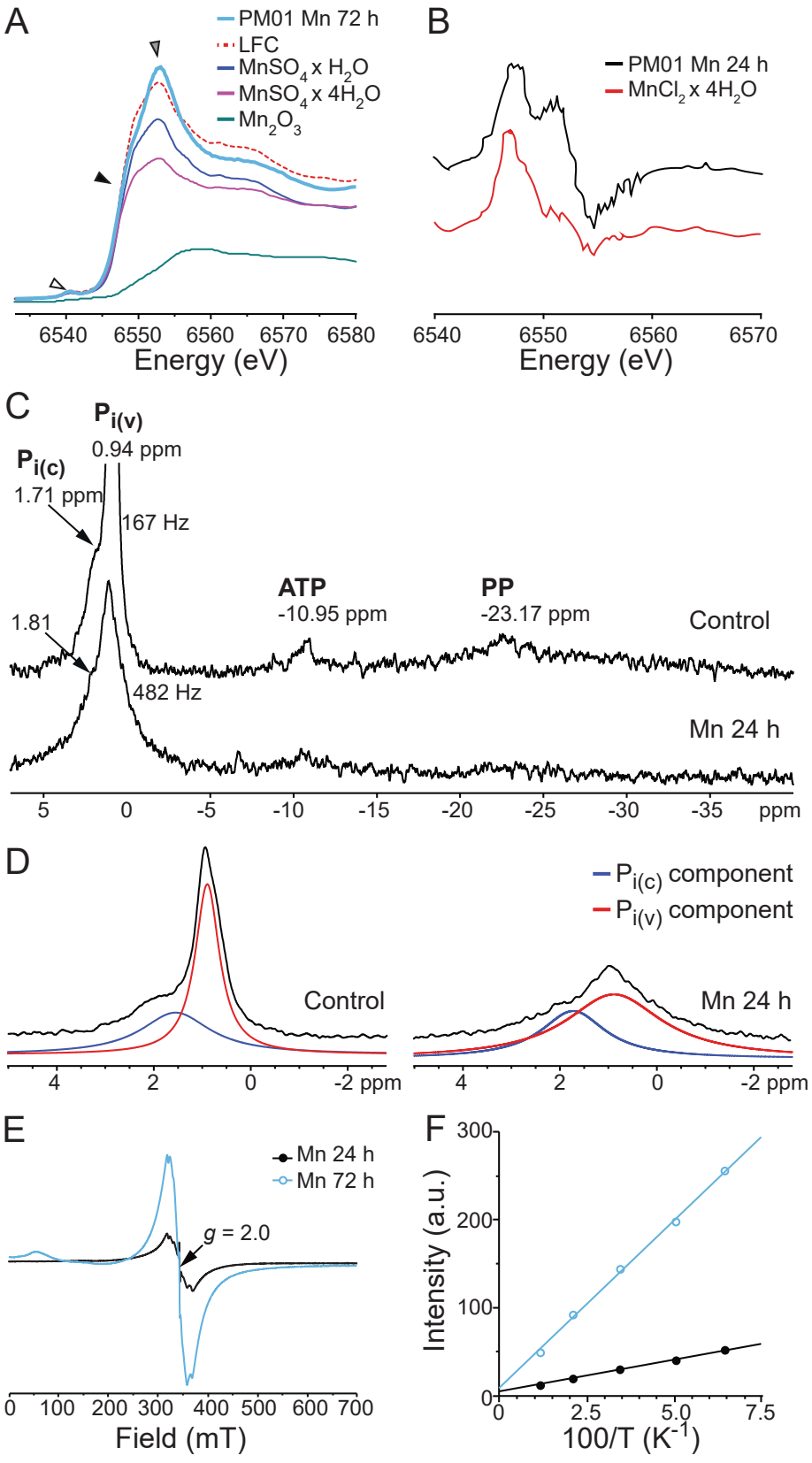

(caption on next page)

Fig. 3. Redox properties and coordination of Mn in *C. acidophila* PM01 biomass. (A) XANES spectra of Mn in *C. acidophila* PM01 biomass (culture was exposed to 20 mM Mn^{2+} for 24 h), and referent Mn^{2+} compounds. Arrowheads: white – pre-edge peak; black – edge peak; gray – 'white line' peak. LFC-linear fitting combination. (B) The comparison of the first derivatives of XANES spectra of Mn in *C. acidophila* PM01 biomass and $MnCl_2{\cdot}4H_2O$. (C) ^{31}P NMR spectra of alive concentrated cultures-untreated or exposed to 2 mM $MnCl_2$ for 24 h. Spectra were collected at 600 MHz and 298 K. Pi – orthophosphate (Pi(c) – in cytosol; Pi(v) – in vacuole); PP – polyphosphates. Chemical shifts (ppm) for all peaks and line widths for Pi(v) peak (Hz; full width at half maximum amplitude) are presented. (D) The results of deconvolution of ^{31}P NMR signal of Pi of control sample and microalgae treated with 2 mM $MnCl_2$ for 24 h. Two signal components were found and assigned to Pi(v) and Pi(c). (E) Room temperature EPR spectra of *C. acidophila* PM01 biomass from cultures treated with 2 mM Mn^{2+} for 24 h or 72 h. (F) Reciprocal-T plot of signal intensity (double integral of EPR signal). It shows straight lines through the origin, which means that the signal intensity follows Curie's law over the indicated temperature range. In the parallel mode no signal was observed. The origin of the low-field signal (around 60 mT) is unknown; it is possibly from a 5-co-ordinate Mn(II). Average spectra (n = 3) are presented.

containing two lines of inorganic (ortho)phosphate (Pi), ATP peak, and a very broad signal of polyphosphates (Nishikawa et al., 2003). It has been

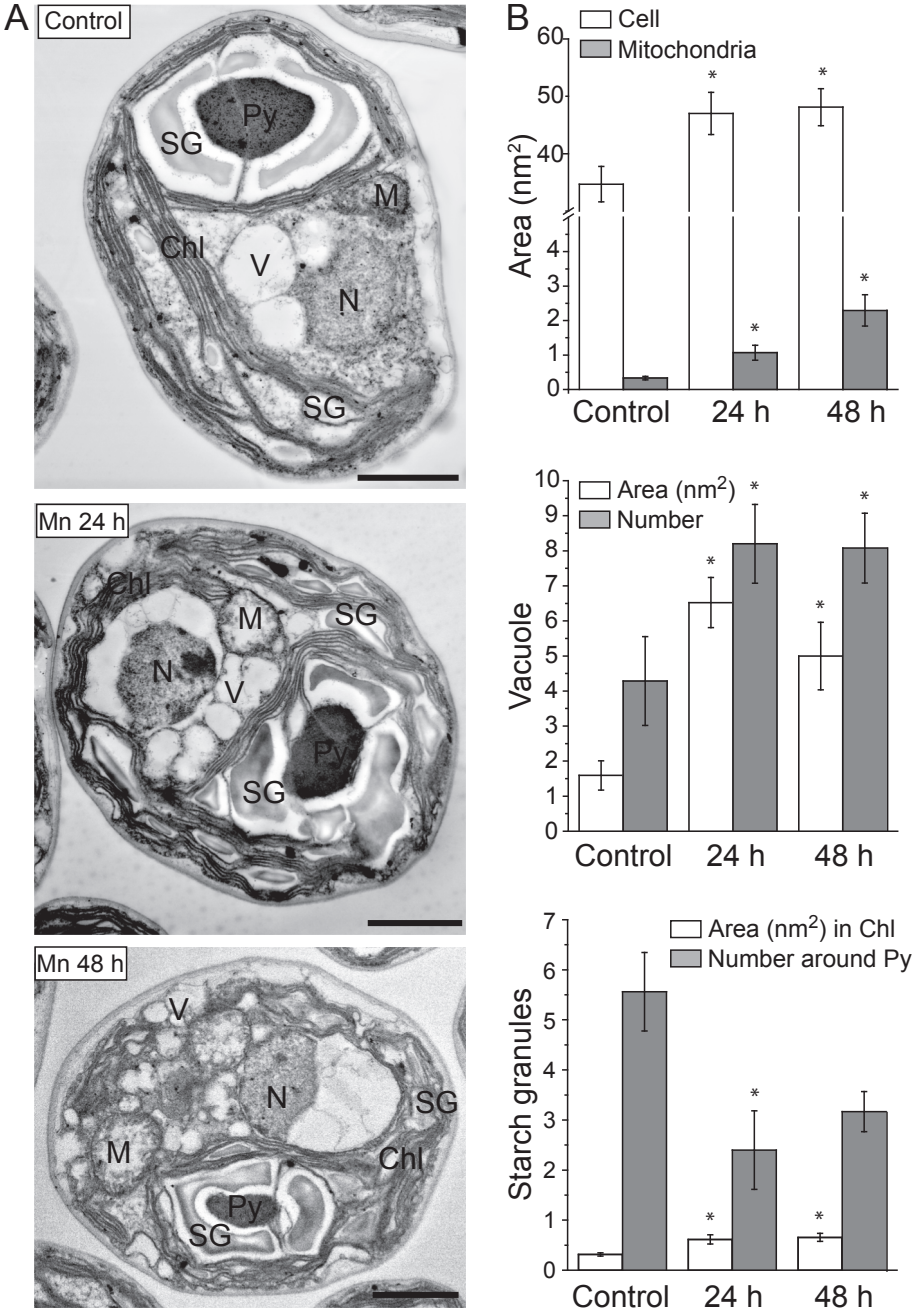

Fig. 4. Representative TEM micrographs and morphometric analysis of *C. acidophila* PM01 cells that were untreated (controls) or treated with 20 mM $MnCl_2$. (A) TEM micrographs. N – nucleus; SG – starch granules (around the pyrenoid (Py) and in the chloroplast (Chl)); V – vacuole; M – mitochondria. Bar – 2 μm. (B) Analysis of TEM micrographs: measurements of total cell and mitochondria area (top panel); area and number of vacuoles (middle panel); and the area of starch granules in the chloroplast and the number of starch granules around pyrenoid (bottom panel). Data are presented as means ± SE (20 cells from n = 3). * – statistically significant compared to control ($p < 0.05$).

shown that the linewidth of polyphosphates signals gain is reduced upon the application of extracellular metal chelator, which implies that these polyphosphates are present in the cell wall, where they are exposed to paramagnetic cations from the culture medium (Nishikawa et al., 2006). The two Pi lines were assigned to Pi in vacuoles and in cytosol according to their chemical shift (Nishikawa et al., 2003; Kuchitsu et al., 1983; Lundberg et al., 1989). To further confirm this, we prepared a pH-dependence curve of ^{31}P NMR chemical shift of orthophosphate (see Supplementary Information). According to this, the peak at $\delta = 1.71$ ppm in controls and $\delta = 1.80$ ppm in treated cells comes from Pi located in the compartment with pH ~6.8 which is appropriate for cytosol, whereas the peak at $\delta = 0.94$ ppm corresponds to Pi at vacuolar pH ~5.7. In cells exposed to Mn, the signal of vacuolar Pi was broadened, probably due to due to interactions with Mn^{2+}, which is a strong paramagnetic. This appears not to be the case with Pi in cytosol, as shown by the deconvolution of Pi signal that separated two signal components (Fig. 3D). This implies that Mn^{2+} is accumulated in vacuoles and that it is coordinated to phosphates, although other ligands, such as organic acids could be present. The addition of Mn^{2+} led to the disappearance of the polyphosphate signal in the cell wall, a known sink for metal ions (Vojvodić et al., 2020), most likely due to binding of paramagnetic Mn ions. In line with XANES analysis, EPR spectroscopy of Mn in the biomass showed a strong signal at $g = 2$ with six-line hyperfine structure (Mn nuclear spin is $I = 5/2$) (Fig. 3C), which is characteristic for Mn^{2+} with weak zero-field interactions and octahedral symmetry (Murali et al., 2005). The hyperfine structure was not well resolved, which implicates a heterogenous coordination geometry. Linear increase in the amplitude of this signal with the inverse of the temperature (Curie's law) is proof that spin system is effectively a two-level system, *i.e.*, it behaves like an electron spin with $S = 1/2$, although Mn^{2+} has $S = 5/2$. In other words, the zero-field interaction energy is much smaller than thermal energy at the lowest operating temperature of 15.5 K. Low zero-field interaction energy is related to octahedral coordination geometry (Eads et al., 1988).

3.4. Changes in cellular structure

Ultrastructural analysis using TEM showed a significant impact of Mn^{2+} (20 mM) on cell structure – disruption of mitochondria, vacuolization, and changes in the size and number of starch granules (Fig. 4). In the majority of cells treated with Mn^{2+}, mitochondria appeared swollen with dissolved matrix and cristae (Fig. 4A). Moderate swelling of mitochondria could be induced by increased energy demands, whereas a severe energy challenge or oxidative stress is known to provoke drastic swelling and a transition of mitochondria to a dysfunctional metabolic state (Javadov et al., 2018). The size of treated cells was also significantly increased (Fig. 4B). Chloroplasts showed no major changes, retaining thylakoid membranes and increasing the size of starch granules, although thylakoid lamellae appeared slightly looser in treated cells (Fig. 4A, B). Mn^{2+} treatment induced a drastic increase in vacuole number and size (Fig. 4B). Vacuoles were located close together in the perinuclear space with the distribution extending to cell periphery in some cells. They appear to fuse as a part of the process of contractile vacuole development (Komsic–Buchmann et al., 2014; Schmollinger et al., 2021). Excretion through contractile vacuoles may be an important mechanism for keeping intracellular Mn levels low. The number of starch granules around the pyrenoid decreased, whereas the size of granules in the chloroplast stroma was increased (Fig. 4B). Although the total number and size of starch granules appeared not to change, biochemical analysis showed an increase in starch content after 24 h of treatment (see Supplementary Information). It has been shown that *peri*-pyrenoid starch granules support the CO_2-concentrating mechanism and improve energy efficiency of the cell (Toyokawa et al., 2020). Therefore, the change in the starch granules around the pyrenoid, along with the mitochondria swelling, may be related to energy challenges that are related to Mn excess. The observed ultrastructural changes, including vacuolization and starch granules accumulation have been reported previously as a part of response to some other heavy metals in different microalgae, including the impact of cadmium on *C. acidophila* cells (Nishikawa et al., 2003; Xiao et al., 2023). Cell wall thickness, pyrenoid size, and nuclear area remained unchanged (data not shown). Moreover, SEM revealed no changes in the shape of algae cells and no mucilage release in response to Mn^{2+} (see Supplementary Information). We noted the presence of vesicle-like structures with diameter of 150–400 nm on the cell surface in all treatments (see Supplementary Information). It has been reported that various microalgal species release extracellular vesicles within this diameter range (Adamo et al., 2024). These vesicles are essential for cell-to-cell communication and adaptation to nutrient stress (Li et al., 2025). The size of extracellular vesicles was increased in response to Mn stress. The presented results imply that PM01 cells may intensify cell-to-cell communication in the time of crisis or use vesicles to release Mn accumulations.

3.5. Changes in the metabolic profile

Changes in the composition of microalgal biomass were examined using SR-μFTIR (Fig. 5). The spectrum was in accord with the previously reported on this strain (Dean et al., 2019; Driver et al., 2015). In the carbohydrate 'fingerprint region' an increase of overall integrate area was observed (Fig. 5D). Bands at 1243, 1151, 1079, 1043 and 1020 cm^{-1} were those that increase the most at 72 h of treatment. These are assigned to several overlapped vibrations: asymmetric stretching of P═O in phosphate groups on phospholipids, phosphorylated carbohydrates and proteins, symmetric stretching of C–—C, C–—O, C–O–—C, and C–O–—P in carbohydrates, and asymmetric stretching of P═O in HPO_4^{2-}. Therefore, the increase of intensity in this region implicates increase in (poly)phosphates or phosphorylation level. The enhancement of bands associated with phosphorus-containing vibrational modes is in line with the proposed Mn accumulation in vacuoles. Protein 'fingerprint' range did not show significant changes. On the other bands assigned to lipids – asymmetric and symmetric stretching of CH_2 and CH_3 group (2925 cm^{-1} and 2854 cm^{-1}, and 2954 and 2873 cm^{-1}), and stretching of H-C═C (3012 cm^{-1}) were weaker in microalgae treated with Mn^{2+}. Biochemical assay showed that the total concentration of lipids was slightly decreased after 48 h (see Supplementary Information). Markers of oxidative stress were observed in both lipids and proteins region. There was a steady increase in the carbonyl signal at ~1730 cm^{-1} which is related to protein oxidation (Fig. 5E). In addition, alkyl chains double bonds signal at 3100–3000 cm^{-1} and the ratio with total lipids significantly decreased upon treatment which implies pronounced lipid peroxidation (Fig. 5F).

3.6. Redox milieu and antioxidative enzymes

The impact of Mn^{2+} on redox milieu was further analyzed using biochemical assays. Intracellular ROS and thiol levels showed reciprocal trends in microalgae treated with Mn^{2+} (Fig. 6A, B). In response to 2 mM Mn^{2+}, ROS concentration showed a peak at 30 min and reached a plateau at 2 h. Such two-step dynamics has been observed previously in *C. sorokiniana* exposed to Mn^{2+} (Vojvodić et al., 2023). The reversibility of early changes in ROS levels is probably related to the increase of thiol concentrations above the physiological level. Thiols in the form of glutathione, phytochelatins and cysteine are an important part of the antioxidative system in microalgae (Pinto et al., 2003). A previous study of the effects of lower concentrations of Mn^{2+} (up to 0.2 mM) on the antioxidative system of microalga *Pavlova viridis* has found significant upregulation of the activity of glutathione peroxidase and total glutathione level (Mei et al., 2007). However, in microalgae treated with 20 mM Mn^{2+}, initial increase of ROS level resulted in an irreversible drop of thiol concentration. Apparently, the exposure to the higher Mn concentration led to oxidative changes that could not be repaired. The development of prooxidative conditions in PM01 could be partially

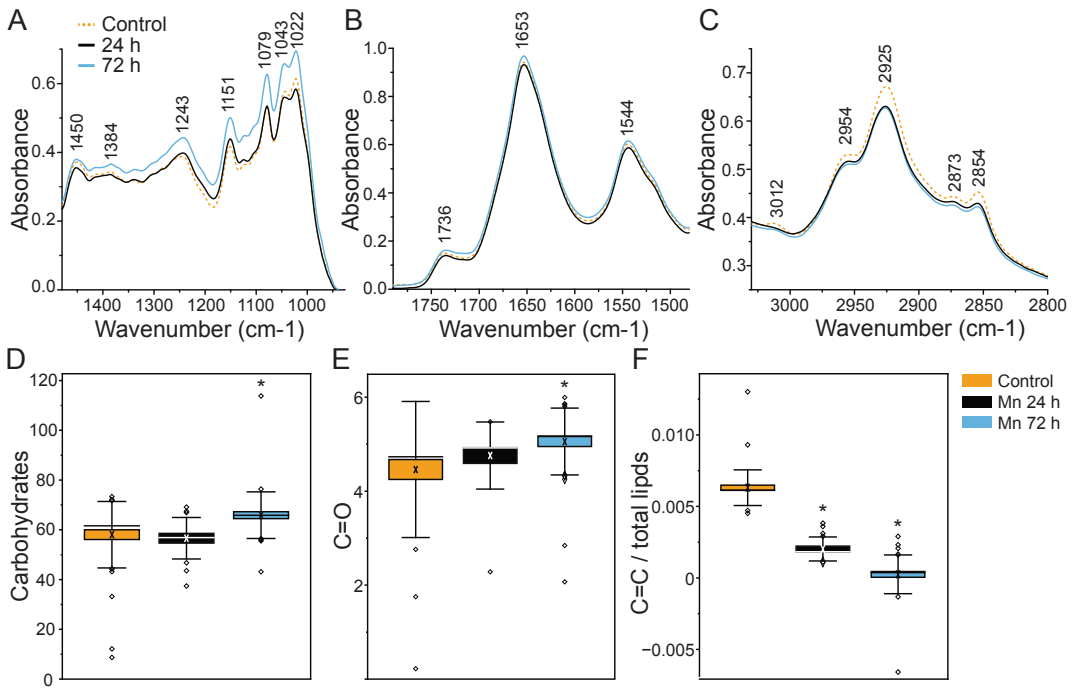

Fig. 5. SR-FTIR analysis of the effects of Mn (20 mM) on the metabolic profile of *C. acidophila* PM01. (A) 'Fingerprint' region for carbohydrates and nucleic acids (1480–900 cm^{-1}); (B) 'Fingerprint' region for proteins (1790–1480 cm^{-1}); (C) 'Fingerprint' region for lipids (3030–2800 cm^{-1}). Arrow – band at 1234 cm^{-1} that is not observable in control. Wavenumbers for bands in control samples are presented. Average spectra (30 spectra from n = 3) are presented. (D) Box plot of the value of the integral values in the 940-1185 cm^{-1} range for carbohydrates; (E) Box plot of the value of the integral values in the 1710-1770 cm^{-1} range for carbonyl. (F) Box plot of the value of the ratio of the integral values of H-C═C stretching and total lipids. Box represents standard error, whiskers standard deviation, horizontal line is the median, cross is the mean, and diamonds are outliers. Data were collected from 30 spectra (n = 3). * – statistically significant differences compared to control ($p < 0.05$).

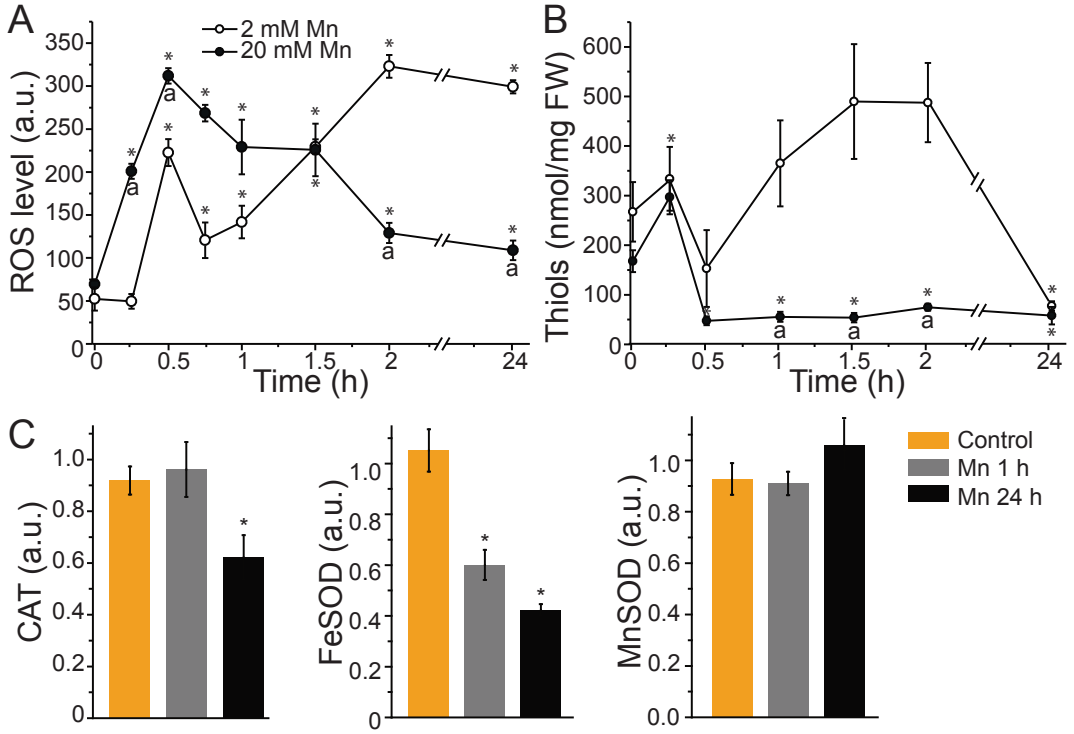

Fig. 6. Redox changes in *C. acidophila* PM01 cells in response to 2 mM or 20 mM $MnCl_2$. (A) Intracellular ROS level evaluated by DCFH fluorescence. a.u.-arbitrary units. (B) Intracellular concentration of reduced thiols. Control values of ROS and reduced thiol levels were determined at 0 h and 24 h; there were no significant differences. Data are presented as mean values ± SE (n = 10). FW – fresh weight. (C) Relative levels (normalized to the band intensity of internal standard GAPDH) of antioxidative enzymes – catalase (CAT) and Fe and Mn superoxide dismutases (FeSOD and MnSOD) that was determined using Western blot. Cells were treated with 20 mM $MnCl_2$. Data are presented as means ± SE (n = 5 for treatments and n = 8 for controls). * – statistically significant differences compared to the initial value at 0 h ($p < 0.05$). [a]-significant compared to 2 mM at the same timepoint.

explained by Mn-induced decrease in the level of Fe-metalloenzymes that are a part of antioxidative defense – FeSOD and catalase (Fig. 6C; see Supplementary Information). The level of MnSOD protein abundance remained unaffected. When present in abundance Mn is known to replace Fe in FeSOD which may be followed by controlled degradation (Diessl et al., 2022; Thompson and Bruick, 2012). Mn could also affect the synthesis of catalase through the competition with Fe for transporters, chaperones and binding sites (Rai et al., 2021), and by decreasing the levels of heme precursors (Yang et al., 2022). Pertinent to the former point, Mn-treated PM01 showed a significant decrease in the intracellular Fe level.

3.7. Photosynthetic performance

Finally, it appears that the exposure to Mn had a slightly positive effects on photosynthetic efficiency (Fig. 7). NPQ was significantly decreased, whereas electron transport rate and resistance to light saturation were modestly improved. NPQ is a protective mechanism for dissipating excess energy from the photosynthetic apparatus which is mediated through lutein and other pigments (Zheng et al., 2022). ETR describes the fraction of photons that are absorbed and 'employed' in carbon fixation (Barranguet and Kromkamp, 2000). Therefore, it appears that Mn improves the performance of the photosynthetic machinery. This is in line with the previous findings that Mn at high concentrations may stimulate photosynthesis in *Chlorella* (Smythers et al., 2023). This is in line with the improved starch content of chloroplasts in cells exposed to Mn^{2+}.

4. Conclusions

The microalga *C. acidophila* PM01 demonstrated physiologically relevant responses to Mn concentrations of up to 20 mM, and survival tolerance to even higher Mn concentrations. This is based on the prevention of intracellular Mn accumulation. We propose, based on indirect observations, that the mechanism behind this includes ionic and coordination binding of significant amounts of Mn^{2+} to the cell wall, and Mn^{2+} vacuolization and sequestration by phosphates, and excretion via contractile vacuolar exocytosis, all of which poses challenges to energy homeostasis (see Supplementary Information). The increased energy demands are met by the consumption of reserves and boosted chloroplast performance. Since Mn pollution does not represent a realistic barrier to *Chlamydomonas acidophila* PM01 growth this strain could be used for commercial exploitation of Mn-infested AMD waters for biomass and biofuels production. On the other hand, the capacity for Mn accumulation is low, so this microalga is not optimal for bioremediation. However, our study points out a novel low-intracellular Mn retention tolerance model that may be specific to acidophilic eukaryotic microalgae. In other words, microalgae tolerate extreme metal concentrations by keeping them out. Some other tolerant normophilic strains, such as *Chlorella sorokiniana* that we have extensively analyzed previously, use a diametral strategy and accumulates and sequesters metals to effectively decrease the extracellular level and unburden ion transporting machinery. However, from the point of survival tolerance, the former strategy is clearly superior. Finally, it is important to clearly state the study's key limitation – laboratory pure culture conditions without in-situ AMD field validation. The proposed strategies of tolerance require further validation on other strains and metals, which represent our main follow-up research direction.

CRediT authorship contribution statement

Isidora Santrač: Writing – original draft, Visualization, Investigation, Formal analysis. **Milena Dimitrijević:** Supervision, Investigation, Formal analysis. **Milan Žižić:** Writing – review & editing, Visualization,

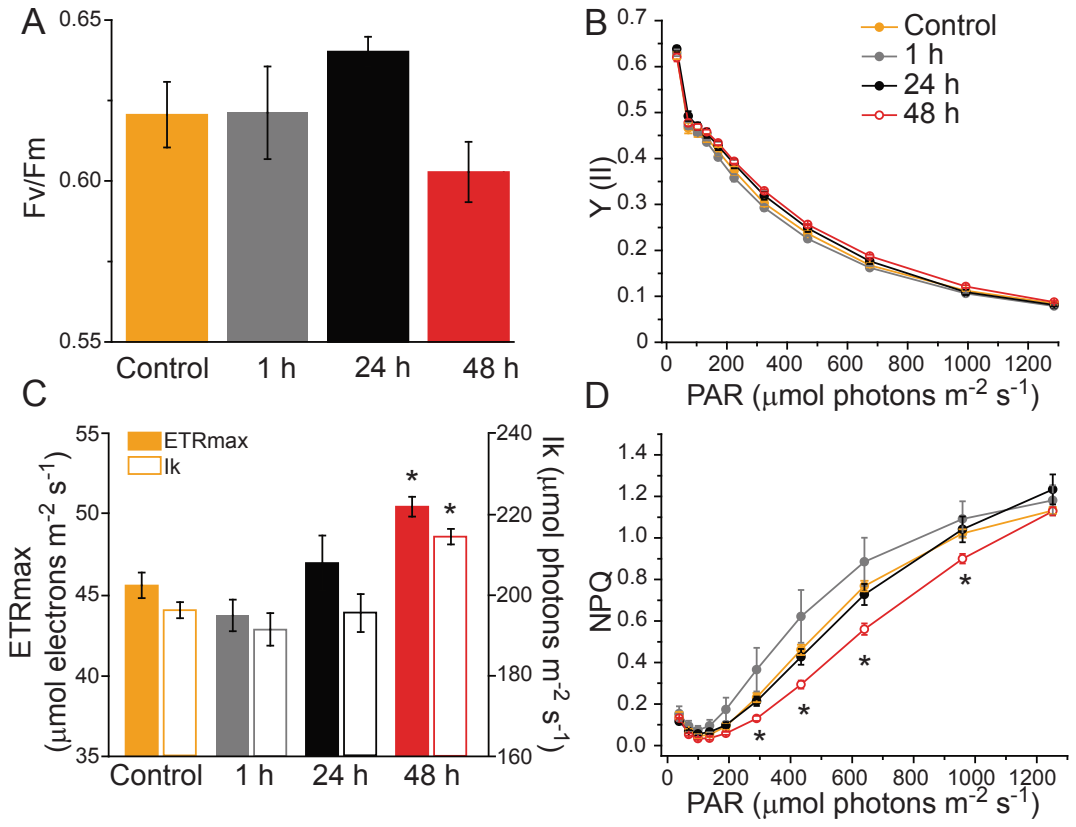

Fig. 7. The effects of Mn^{2+} on the photosynthetic properties of *C. acidophila* PM01. Cells were treated with 20 mM. (A) Maximum quantum yield of PSII (Fv/Fm). (B) Effective photosynthetic yield, Y(II). (C) Maximum electron transport rate, ETRmax; and minimum saturating irradiance, Ik. (d) Non-photochemical quenching, NPQ. Data are presented as means ± SE (n = 10). * – statistically significant differences compared to control ($p < 0.05$).

Methodology, Investigation, Formal analysis. **Marina Stanić:** Investigation, Formal analysis. **Valentina Ćurić:** Investigation, Formal analysis. **Valentina Bonanni:** Methodology, Formal analysis, Data curation. **Alessandra Gianoncelli:** Methodology, Formal analysis, Data curation. **Giuliana Aquilanti:** Methodology, Formal analysis, Data curation. **Chiaramaria Stani:** Methodology, Formal analysis, Data curation. **Giovanni Birarda:** Methodology, Formal analysis, Data curation. **Wilfred Hagen:** Methodology, Formal analysis, Data curation. **Uroš Javornik:** Methodology, Formal analysis, Data curation. **Bernd Zechmann:** Writing – review & editing, Methodology, Formal analysis, Data curation. **Jon K. Pittman:** Writing – review & editing, Data curation. **Ivan Spasojević:** Writing – original draft, Visualization, Supervision, Project administration, Conceptualization. **Jelena Danilović Luković:** Writing – original draft, Visualization, Supervision.

Declaration of competing interest

The authors declare that they have no known competing financial interests or personal relationships that could have appeared to influence the work reported in this paper.

Acknowledgement

This research was financially supported by the Science Fund of the Republic of Serbia, #7078, Microalgae for biosynthesis of metal cluster compounds – BioSynthClust. We gratefully acknowledge the financial support provided by the International Atomic Energy Agency (IAEA) through the IAEA Collaborating Centre at Elettra Sincrotrone Trieste for Project No. 20240306, carried out at the XRF beamline of the Elettra synchrotron facility. The authors acknowledge the CERIC-ERIC Consortium for the access to experimental facilities (project n. 20237234 - beamline SISSI at Elettra, and project n. 20242098 - Slovenian NMR center) and for the financial support for both projects. The research leading to this result (proposal n. 20240044) has been co-funded by the project NEPHEWS under Grant Agreement No 101131414 from the EU Framework Programme for Research and Innovation Horizon Europe. Views and opinions expressed are however those of the author(s) only and do not necessarily reflect those of the European Union. Neither the European Union nor the Granting Authorities can be held responsible for them. The authors also acknowledge the support of COST Action CA21115.

Appendix A. Supplementary data

Supplementary data to this article can be found online at https://doi.org/10.1016/j.biortech.2026.135510.

Data availability

Data will be made available on request.

References

Adamo, G., Santonicola, P., Picciotto, S., Gargano, P., Nicosia, A., Longo, V., Aloi, N., Romancino, D.P., Paterna, A., Rao, E., Raccosta, S., 2024. Extracellular vesicles from the microalga Tetraselmis chuii are biocompatible and exhibit unique bone tropism along with antioxidant and anti−inflammatory properties. Comm. Biol. 7 (1), 941.

Alho, L.D.O.G., Gebara, R.C., Mansano, A.D.S., Rocha, G.S., Melão, M.D.G.G., 2022. Individual and combined effects of manganese and chromium on a freshwater Chlorophyceae. Environ. Toxicol. Chem. 41 (4), 1004–1015.

Barranguet, C., Kromkamp, J., 2000. Estimating primary production rates from photosynthetic electron transport in estuarine microphytobenthos. Mar. Ecol. Prog. Ser. 204, 39–52.

Birarda, G., Bedolla, D., Piccirilli, F., Stani, C., Vondracek, H., Vaccari, L., 2022. Chemical analyses at micro and nano scale at SISSI−Bio beamline at Elettra−Sincrotrone Trieste. Proc SPIE 11957. Biomedical Vibrational Spectroscopy 2022: Advances in Research and Industry.

Blaby-Haas, C.E., Merchant, S.S., 2012. The ins and outs of algal metal transport. BBA 1823 (9), 1531–1552.

Blumwald, E., Aharon, G.S., Apse, M.P., 2000. Sodium transport in plant cells. Biochim. Biophys. Acta Biomemb. 1465 (1–2), 140–151.

Canadian Phycological Culture Centre, 2026. Modified Acid Medium (MAM). https://uwaterloo.ca/canadian−phycological−culture−centre/cultures/culture−media/modified−acid−medium (Accessed on February 26th, 2026).

Cândido, G.C., Santos, A.A., Santiago, A.F., Leão, V.A., 2024. Insights into manganese removal from mine water by Chlorella vulgaris. Int. J. Environ. Sci. Technol. 21 (5), 4715–4726.

Cazzaniga, S., Dall'Osto, L., Szaub, J., Scibilia, L., Ballottari, M., Purton, S., Bassi, R., 2014. Domestication of the green alga Chlorella sorokiniana: reduction of antenna size improves light−use efficiency in a photobioreactor. Biotechnol. Biofuels 7 (1), 157.

Dean, A.P., Hartley, A., McIntosh, O.A., Smith, A., Feord, H.K., Holmberg, N.H., King, T., Yardley, E., White, K.N., Pittman, J.K., 2019. Metabolic adaptation of a Chlamydomonas acidophila strain isolated from acid mine drainage ponds with low eukaryotic diversity. Sci. Total Environ. 647, 75–87.

Dey, S., Tripathy, B., Kumar, M.S., Das, A.P., 2023. Ecotoxicological consequences of manganese mining pollutants and their biological remediation. Environ. Chem. Ecotoxicol. 5, 55–61.

Diessl, J., Berndtsson, J., Broeskamp, F., Habernig, L., Kohler, V., Vazquez-Calvo, C., Nandy, A., Peselj, C., Drobysheva, S., Pelosi, L., Vögtle, F.N., 2022. Manganese−driven CoQ deficiency. Nat. Comm. 13 (1), 6061.

Driver, T., Bajhaiya, A.K., Allwood, J.W., Goodacre, R., Pittman, J.K., Dean, A.P., 2015. Metabolic responses of eukaryotic microalgae to environmental stress limit the ability of FT−IR spectroscopy for species identification. Algal Res. 11, 148–155.

Eads, C.D., LoBrutto, R., Kumar, A., Villafranca, J.J., 1988. Identification of nonprotein ligands to the metal ions bound to glutamine synthetase. Biochemistry 27 (1), 165–170.

Gianoncelli, A., Bonanni, V., Gariani, G., Guzzi, F., Pascolo, L., Borghes, R., Billè, F., Kourousias, G., 2021. Soft X−ray microscopy techniques for medical and biological imaging at TwinMic—Elettra. Appl. Sci. 11 (16), 7216.

Gianoncelli, A., Kourousias, G., Merolle, L., Altissimo, M., Bianco, A., 2016. Current status of the TwinMic beamline at Elettra: a soft X−ray transmission and emission microscopy station. J. Synchrotron Radiat. 23 (Pt 6), 1526–1537.

Gianoncelli, A., Morrison, G.R., Kaulich, B., Bacescu, D., Kovac, J., 2006. Scanning transmission x−ray microscopy with a configurable detector. Appl. Phys. Lett. 89 (25), 251117.

Haberman, K.L., Lukovic, J.D., Kovacevic, S., Zhang, X., Kebaara, B., Taube, J., Berti, D., Zechmann, B., 2025. Comprehensive comparison between STEM−HAADF and TEM bright−field mode for imaging resin embedded biological samples. Microsc. Microanal. 31 (3), ozaf038.

Imlay, J.A., 2014. The mismetallation of enzymes during oxidative stress. J. Biol. Chem. 289 (41), 28121–28128.

Javadov, S., Chapa-Dubocq, X., Makarov, V., 2018. Different approaches to modeling analysis of mitochondrial swelling. Mitochondrion 38, 58–70.

Kalyanaraman, B., Darley-Usmar, V., Davies, K.J., Dennery, P.A., Forman, H.J., Grisham, M.B., Mann, G.E., Moore, K., Roberts II, L.J., Ischiropoulos, H., 2012. Measuring reactive oxygen and nitrogen species with fluorescent probes: challenges and limitations. Free Radic. Biol. Med. 52 (1), 1–6.

Karydas, A.G., Czyzycki, M., Leani, J.J., Migliori, A., Osan, J., Bogovac, M., Wrobel, P., Vakula, N., Padilla-Alvarez, R., Menk, R.H., Gol, M.G., Antonelli, M., Tiwari, M.K., Caliri, C., Vogel-Mikuš, K., Darby, I., Kaiser, R.B., 2018. An IAEA multi-technique X-ray spectrometry endstation at Elettra Sincrotrone Trieste: Benchmarking results and interdisciplinary applications. J. Synchrotron Radiat. 25, 189–203.

Khramtsov, V.V., Yelinova, V.I., Weiner, L.M., Berezina, T.A., Martin, V.V., Volodarsky, L.B., 1989. Quantitative determination of SH groups in low−and high−molecular−weight compounds by an electron spin resonance method. Anal. Biochem. 182 (1), 58–63.

Komsic-Buchmann, K., Wöstehoff, L., Becker, B., 2014. The contractile vacuole as a key regulator of cellular water flow in *Chlamydomonas reinhardtii*. Eukaryot. Cell. 13 (11), 1421–1430.

Kossoff, D., Dubbin, W.E., Alfredsson, M., Edwards, S.J., Macklin, M.G., Hudson-Edwards, K.A., 2014. Mine tailings dams: characteristics, failure, environmental impacts. Appl. Geochem. 51, 229–245.

Kourousias, G., Guzzi, F., Pugliese, R., Billè, F., Tsampa, K., Gianoncelli, A., 2026. XRFitVis: a cloud−based visualization tool for μXRF mapping datasets. X−ray Spectrometr. 55 (1), 76–82.

Kuchitsu, K., Oh-hama, T., Tsuzuki, M., Miyachi, S., 1983. Detection and characterization of acidic compartments (vacuoles) in Chlorella vulgaris 11h cells by 31P-in vivo NMR spectroscopy and cytochemical techniques. Arch. Microbiol. 148, 83–87.

Lacerda, S., Ndiaye, D., Tóth, É., 2021. MRI relaxation agents based on transition metals. Adv. Inorg. Chem. 78, 109–142.

Li, C., Zhu, R., Chen, Z., Du, M., Liu, Y., Liu, C., Jiang, P., Luo, Y., Lei, A., Liu, Q., Zhu, H., 2025. Extracellular vesicles in *Chlamydomonas reinhardtii*: Mediators of nutrient sensing and cell−to−cell communication. Algal Res. 85, 103853.

Li, M., Zhu, Q., Hu, C.W., Chen, L., Liu, Z.L., Kong, Z.M., 2007. Cobalt and manganese stress in the microalga Pavlova viridis (Prymnesiophyceae): effects on lipid peroxidation and antioxidant enzymes. J. Environ. Sci. 19 (11), 1330–1335.

Li, Y., Xu, Z., Ma, H., Hursthouse, S.A., 2019. Removal of manganese (II) from acid mine wastewater: a review of the challenges and opportunities with special emphasis on Mn−oxidizing bacteria and microalgae. Water. 11 (12), 2493.

Li, Y., Zhou, C., Chen, L., Deng, R., Wong, M., Shan, S., 2024. Effects of biochar on the manganese enrichment and oxidation by a microalga Scenedesmus quadricauda in the aquatic environment. Ecotoxicol. Environ. Saf. 271, 115961.

Liu, J., Tan, K., He, L., Qiu, Y., Tan, W., Guo, Y., Wang, Z., Sun, W., 2018. Effect of limitation of iron and manganese on microalgae growth in fresh water. Microbiology. 164 (12), 1514–1521.
Long, H., Fang, J., Ye, L., Zhang, B., Hui, C., Deng, X., Merchant, S.S., Huang, K., 2023. Structural and functional regulation of Chlamydomonas lysosome−related organelles during environmental changes. Plant Physiol. 192 (2), 927–944.
Lundberg, P., Weich, R.G., Jensén, P., Vogel, H.J., 1989. Phosphorus-31 and nitrogen- 14 NMR studies of the uptake of phosphorus and nitrogen compounds in the marine macroalgae Ulva lactuca. Plant Physiol. 89 (4), 1380–1387.
Marczenko, Z., Balcerzak, M., 2000. Separation, Preconcentration and Spectrophotometry in Inorganic Analysis. Elsevier, Amsterdam.
Mcintosh, O.A., 2021. A broad study of the extremophile Chlamydomonas acidophila, isolated from an abandoned copper mine in Parys Mountain. The University of Manchester, Manchester. PhD Thesis.
Mei, L.I., Qin, Z.H.U., Chang-Wei, H., Li, C.H.E.N., Zhi-Li, L., Zhi-Ming, K., 2007. Cobalt and manganese stress in the microalga Pavlova viridis (Prymnesiophyceae): effects on lipid peroxidation and antioxidant enzymes. J. Environ. Sci. 19 (11), 1330–1335.
Movasaghi, Z., Rehman, S., Rehman, I., 2008. Fourier transform infrared (FTIR) spectroscopy of biological tissues. Appl. Spectros. Rev. 43 (2), 134–179.
Murali, A., Chakradhar, R.S., Rao, J.L., 2005. Allowed and forbidden hyperfine structure of Mn2+ ions in sodium tetraborate glasses—an EPR and optical study. Physica B: Condens. Matter 358 (1–4), 19–26.
Ňancucheo, I., Johnson, D.B., 2011. Significance of microbial communities and interactions in safeguarding reactive mine tailings by ecological engineering. Appl. Environ. Microbiol. 77 (23), 8201–8208.
Neculita, C.M., Rosa, E., 2019. A review of the implications and challenges of manganese removal from mine drainage. Chemosphere 214, 491–510.
Nishikawa, K., Machida, H., Yamakoshi, Y., Ohtomo, R., Saito, K., Saito, M., Tominaga, N., 2006. Polyphosphate metabolism in an acidophilic alga Chlamydomonas acidophila KT−1 (Chlorophyta) under phosphate stress. Plant Sci. 170 (2), 307–313.
Nishikawa, K., Yamakoshi, Y., Uemura, I., Tominaga, N., 2003. Ultrastructural changes in Chlamydomonas acidophila (Chlorophyta) induced by heavy metals and polyphosphate metabolism. FEMS Microbiol. Ecol. 44 (2), 253–259.
Nixdorf, B., Mischke, U., Leßmann, D., 1998. Chrysophytes and chlamydomonads: pioneer colonists in extremely acidic mining lakes (pH< 3) in Lusatia (Germany). Hydrobiologia. 369, 315–327.
Nowicka, B., 2022. Heavy metal−induced stress in eukaryotic algae−mechanisms of heavy metal toxicity and tolerance with particular emphasis on oxidative stress in exposed cells and the role of antioxidant response. Environ. Sci. Pollut. Res. Int. 29 (12), 16860–16911.
Olaveson, M.M., Stokes, P.M., 1989. Responses of the acidophilic alga Euglena mutabilis (Euglenophyceae) to carbon enrichment at pH 3. J. Phycol. 25 (3), 529–539.
Olsson, S., Puente-Sanchez, F., Gómez, M.J., Aguilera, A., 2015. Transcriptional response to copper excess and identification of genes involved in heavy metal tolerance in the extremophilic microalga Chlamydomonas acidophila. Extremophiles 19 (3), 657–672.
Pinto, E., Sigaud-Kutner, T.C., Leitao, M.A., Okamoto, O.K., Morse, D., Colepicolo, P., 2003. Heavy metal–induced oxidative stress in algae 1. J. Phycol. 39 (6), 1008–1018.
Platt, T., Gallegos, C.L., Harrison, W.G., 1980. Photoinhibition of photosynthesis in natural assemblages of marine phytoplankton. J. Mar. Res. 38 (4), 687–701.
Pittman, J.K., 2005. Managing the manganese: molecular mechanisms of manganese transport and homeostasis. New Phytol. 167 (3), 733–742.
Puente-Sánchez, F., Díaz, S., Penacho, V., Aguilera, A., Olsson, S., 2018. Basis of genetic adaptation to heavy metal stress in the acidophilic green alga Chlamydomonas acidophila. Aquat. Toxicol. 200, 62–72.
Rai, S., Singh, P.K., Mankotia, S., Swain, J., Satbhai, S.B., 2021. Iron homeostasis in plants and its crosstalk with copper, zinc, and manganese. Plant Stress 1, 100008.
Ravel, B., Newville, M., 2005. ATHENA, ARTEMIS, HEPHAESTUS: data analysis for X−ray absorption spectroscopy using IFEFFIT. Synchrotron Radiat. 12 (4), 537–541.
Saha, S.K., Moane, S., Murray, P., 2013. Effect of macro−and micro−nutrient limitation on superoxide dismutase activities and carotenoid levels in microalga Dunaliella salina CCAP 19/18. Bioresour. Technol. 147, 23–28.
Schmollinger, S., Chen, S., Merchant, S.S., 2023. Quantitative elemental imaging in eukaryotic algae. Metallomics. 15 (5), mfad025.
Schmollinger, S., Chen, S., Strenkert, D., Hui, C., Ralle, M., Merchant, S.S., 2021. Single−cell visualization and quantification of trace metals in Chlamydomonas lysosome−related organelles. Proc. Nat. Acad. Sci. USA 118 (16), e2026811118.
Shanab, S., Essa, A., Shalaby, E., 2012. Bioremoval capacity of three heavy metals by some microalgae species (Egyptian Isolates). Plant Signal. Behav. 7 (3), 392–399.
Shu, J., Liu, R., Liu, Z., Chen, H., Tao, C., 2016. Simultaneous removal of ammonia and manganese from electrolytic metal manganese residue leachate using phosphate salt. J. Clean. Prod. 135, 468–475.
Sim, L.N., Ho, J.S., Khaswan, N.B., Wu, B., Chong, T.H., 2021. Membrane filtration of manganese (II) remediated−microalgae: manganese (II) removal, extracellular organic matter, and membrane fouling. Algal Res. 55, 102279.
Smythers, A.L., Crislip, J.R., Slone, D.R., Flinn, B.B., Chaffins, J.E., Camp, K.A., McFeeley, E.W., Kolling, D.R., 2023. Excess manganese increases photosynthetic activity via enhanced reducing center and antenna plasticity in Chlorella vulgaris. Sci. Rep. 13 (1), 11301.
Smythers, A.L., Perry, N.L., Kolling, D.R., 2019. Chlorella vulgaris bioaccumulates excess manganese up to 55× under photomixotrophic conditions. Algal Res. 43, 101641.
Solé, V.A., Papillon, E., Cotte, M., Walter, P., Susini, J., 2007. A multiplatform code for the analysis of energy−dispersive X−ray fluorescence spectra. Spectrochim. Acta Part b: at. Spectrosc. 62 (1), 63–68.
Tanović, M., Žižić, M., Milenković, M., Jagličić, Z., Hagen, W., Stanić, M., Stanković, D., Kovačević, S., Karpov, D., Šket, P., Javornik, U., Spasojević, I., Dimitrijević, M., 2025. Employing microalga Chlorella sorokiniana in the biosynthesis of paramagnetic and catalytically functional manganese cluster. Bioresour. Technol. 432, 132692.
Thompson, J.W., Bruick, R.K., 2012. Protein degradation and iron homeostasis. Biochim. Biophys. Acta Mol. Cell Res. 1823 (9), 1484–1490.
Toplak, M., Birarda, G., Read, S., Sandt, C., Rosendahl, S.M., Vaccari, L., Demšar, J., Borondics, F., 2017. Infrared orange: connecting hyperspectral data with machine learning. Synchrotron Radiat. News 30 (4), 40–45.
Toplak, M., Read, S.T., Sandt, C., Borondics, F., 2021. Quasar: easy machine learning for biospectroscopy. Cells 10 (9), 2300.
Toyokawa, C., Yamano, T., Fukuzawa, H., 2020. Pyrenoid starch sheath is required for LCIB localization and the CO2−concentrating mechanism in green algae. Plant Physiol. 182 (4), 1883–1893.
Vasilieva, S.G., Gorelova, O.A., Baulina, O.I., Lobakova, E.S., 2022. Subcellular localization of manganese in two green microalgae species with different tolerance to elevated Mn concentrations. Russ. J. Plant Physiol. 69 (5), 94.
Vojvodić, S., Danilović Luković, J., Zechmann, B., Jevtović, M., Bogdanović Pristov, J., Stanić, M., Lizzul, A.M., Pittman, J.K., Spasojević, I., 2020. The effects of ionizing radiation on the structure and antioxidative and metal−binding capacity of the cell wall of microalga Chlorella sorokiniana. Chemosphere 260, 127553.
Vojvodić, S., Dimitrijević, M., Žižić, M., Dučić, T., Aquilanti, G., Stanić, M., Zechmann, B., Danilović Luković, J., Stanković, D., Opačić, M., Morina, A., Pittman, J.K., Spasojević, I., 2023. A three−step process of manganese acquisition and storage in the microalga Chlorella sorokiniana. J. Exp. Bot. 74 (3), 1107–1122.
Walz, H., 2000. WinControl—Windows software for PAM Fluorometers users manual. Heinz Walz GmbH, Effeltrich.
Wibowo, Y.G., Safitri, H., Kusumawati, Aini, W.D., Farantino, R., Ginting, S.B., Rinovian, A., Kurniawan, S.B., Khairurrijal, K., Taher, T., Kusumaningrum, W.B., Sudibyo, S., Yuliansyah, A.T., Petrus, H.T.B.M., 2025. Biochar MMT ZnAl LDH composite materials derived from solid waste for heavy metal removal in artificial acid mine drainage. Sci. Rep. 15 (1), 14914.
Wollmann, F., Dietze, S., Ackermann, J.U., Bley, T., Walther, T., Steingroewer, J., Krujatz, F., 2019. Microalgae wastewater treatment: biological and technological approaches. Eng. Life Sci. 19 (12), 860–871.
Xiao, X., Li, W., Jin, M., Zhang, L., Qin, L., Geng, W., 2023. Responses and tolerance mechanisms of microalgae to heavy metal stress: a review. Mar. Environ. Res. 183, 105805.
Yang, S., Ling, G., Li, Q., Yi, K., Tang, X., Zhang, M., Li, X., 2022. Manganese toxicity−induced chlorosis in sugarcane seedlings involves inhibition of chlorophyll biosynthesis. Crop J. 10 (6), 1674–1682.
Zheng, H., Wang, Y., Li, S., Nagarajan, D., Varjani, S., Lee, D.J., Chang, J.S., 2022. Recent advances in lutein production from microalgae. Renew. Sustain. Energy Rev. 153, 111795.
Zuppini, A., Andreoli, C., Baldan, B., 2007. Heat stress: an inducer of programmed cell death in Chlorella saccharophila. Plant Cell Physiol. 48 (7), 1000–1009.